ORIGINAL ARTICLE

Spectroscopic Methodology

Whole brain ^{31}P MRSI at 7T with a dual-tuned receive array

Benjamin C. Rowland[1, 2] | Ian D. Driver[2] | Mohamed Tachrount[2] | Dennis W. J. Klomp[3, 4] | Debra Rivera[4] | Ria Forner[4] | Anh Pham[4] | Michel Italiaander[4] | Richard G. Wise[2]

[1]Division of Cancer Science, University of Manchester, Manchester, UK

[2]Cardiff University Brain Research Imaging Centre, School of Psychology, Cardiff University, Cardiff, UK

[3]Radiology, UMC Utrecht, Utrecht, Netherlands

[4]MR Coils, Zaltbommel, Netherlands

Correspondence
Benjamin C. Rowland, Division of Cancer Science, University of Manchester, Manchester, M13 9PL, UK
Email: benjamin.rowland@manchester.ac.uk

Funding information
Word Count: 4301

Purpose: The design and performance of a novel head coil setup for ^{31}P spectroscopy at ultra high field strengths (7T) is presented. The described system supports measurements at both the ^{1}H and ^{31}P resonance frequencies.

Methods: The novel coil consists of two, actively detunable, coaxial birdcage coils to give homogeneous transmit, combined with a double resonant 30 channel receive array. This allows for anatomical imaging combined with ^{31}P acquisitions over the whole head, without changing coils or disturbing the subject.

A phosphate buffer phantom and three healthy volunteers were scanned with a pulse acquire CSI sequence using both the novel array coil and a conventional transceiver birdcage. Four different methods of combining the array channels were compared at three different levels of SNR.

Results: The novel coil setup delivers significantly increased ^{31}P SNR in the peripheral regions of the brain, reaching up to factor 8, while maintaining comparable performance relative to the birdcage in the center.

Conclusions: The new system offers the potential to acquire whole brain ^{31}P MRSI with superior signal relative to the standard options.

KEYWORDS
MRSI, ^{31}P, phosphorus, spectroscopy, dual-tuned, receive array

1 | INTRODUCTION

Magnetic resonance spectroscopy of the ^{31}Phosphorus nucleus can be used to explore several interesting metabolic processes *in vivo*, including energy metabolism, cell membrane turnover, and intra- and extra-cellular pH[1, 2, 3, 4]. However, there are many challenges to acquiring high quality phosphorus spectra, particularly the low sensitivity of the ^{31}P nucleus relative to ^{1}H, and the generally low concentrations of the metabolites of interest, which result in low signal-to-noise ratio (SNR). Working at ultra-high field strengths offers a considerable boost to signal strength, for example Rodgers *et al.* found a super-linear increase of 2.8x sensitivity in the heart when moving from 3T to 7T[5]. At the same time, the phosphorus nucleus is not as susceptible to the issues that affect proton MR at UHF, such as B_1 inhomogeneity. In addition, the increased spectral dispersion at UHF allows resolving closely spaced peaks, such as phosphocholine (PC) and phosphoethanolamine (PE), which would be extremely challenging to distinguish at lower field strengths. For these reasons, the move to higher field strengths is particularly advantageous for ^{31}P MRS.

The difference in Larmor frequencies between ^{1}H and ^{31}P means that purpose-built hardware is required to acquire phosphorus spectra. The design of that hardware is critical to its performance. For example, multi-receiver arrays of surface coils provide excellent SNR close to individual elements, but with limited field of view. When used to transmit RF, they also have an inhomogeneous B_1^+: to achieve a uniform excitation therefore requires the use of adiabatic pulses, with a corresponding substantial increase in SAR. By contrast, volume coils have a much more homogeneous B_1, both for transmit and receive. A common solution to these limitations is to use a combined design, with a volume coil used for transmit in order to allow short, low SAR excitation pulses, together with an array of receivers to benefit from the improved SNR[6].

Another issue to consider in designing a ^{31}P coil is the need to also incorporate a separate ^{1}H system[7]. This is necessary to provide standard anatomical imaging for accurate localization of the ^{31}P signals, and also offers the potential to investigate the relationships between ^{1}H and ^{31}P functional results. While it is relatively straightforward to add a ^{1}H volume coil outside the ^{31}P setup, this severely limits the potential of the coil for more advanced proton imaging, relative to a typical multi-channel array. At 7T, where significant calibration is often necessary for each exam, it is not practical to change coils mid-exam, even disregarding the challenges of registering data from the two parts. It would be greatly preferable for the ^{1}H imaging to use a dual-tuned receiver array so that both nuclei can benefit from the improvements to SNR, however it remains an open question how much such dual-tuning will reduce the already low ^{31}P SNR.

In this study, we examine the performance of a novel coil setup, built by MR Coils (Zaltbommel, Netherlands) designed for whole head ^{1}H and ^{31}P MR. It combines individual volume coils for transmit at both ^{1}H and ^{31}P frequencies with a close-fitting, 30 channel, dual-tuned receiver array. This novel coil design was benchmarked against a conventional quadrature volume coil.

When combining the individual channels of the array coil, the correct choice of weightings is essential to obtain optimal final signal quality. Rodgers *et al.* showed that in practice data driven methods generally achieve the best weightings, providing sufficient SNR is available. In ^{1}H MRS, there is generally plenty of SNR, which makes calculating the channel weights fairly straightforward. However, in the relatively SNR poor phosphorus case, there is a danger that the calculated weights are not optimal, which in turn further reduces the final SNR of the combined signal. Here, we consider various state-of-the-art combination strategies applied to different datasets with varying levels of intrinsic

SNR, to evaluate their relative performance under these challenging conditions.

2 | METHODS

2.1 | Coil Design

Volume transmit system

A design similar to that proposed by J. R. Fitzsimmons *et al.*[8] was chosen, with two birdcage coils situated co-axially. The primary goal for the transmit birdcages was dual resonance, optimized for ^{31}P, with a secondary goal of unhampered visibility for the subject to allow visual stimuli and instructions to be presented. To accomplish this ceramic cable traps were used to suppress common-mode currents on the cables.

The inner birdcage layer with a radius of 12.5 cm was first tuned to 120.6 MHz (^{31}P at 7T) under conditions of symmetry. In addition, traps tuned to 297.8 MHz (^{1}H at 7T) were placed on each of the legs to avoid losses arising from the counter-currents at the two frequencies, a problem inherent in many other dual-tuned birdcage designs. The outer birdcage with a radius of 14.25 cm was tuned to the ^{1}H frequency in isolation. Since the operation of the higher frequency was not significantly affected by the presence of the lower frequency birdcage (including the traps), no traps were necessary. The lower frequency birdcage was then introduced inside and the traps were adjusted to decouple it from the ^{1}H birdcage, which restored the ^{31}P resonance frequency, meaning that no adjustment of the tuning capacitors was required.. Both birdcages were 12 cm long (Figure 1e).

The bird-cages were originally designed to separate into two pieces to facilitate subject positioning, however this process was found to create too much variation in the coil matching, so the birdcages were returned to a single piece. Both birdcages were made detunable by means of PIN diodes placed in parallel to the (33pF for ^{31}P and 2.7pF for ^{1}H) capacitors on one end-ring.

In order to allow the subject to receive visual stimuli, a rectangular window was cut through the lower half of the anterior portion; which was mirrored with a window of the same dimensions, diagonally across, on the upper half of the posterior section. The window was then covered with a mesh shield (50dB EMV Abschirmstoff Aaronia-Shield ®, Aaronia AG, Eifel Germany), to restore its shielding properties while allowing visibility out of the coil (Figure 1d).

The cables at the two ports for each birdcage were then added and fine-adjusted by changing the length of copper trace between the inner and outer conductors to minimise reflection co-efficients. Shield currents along the co-axial cables were mitigated by means of ceramic floating cable traps; placed close to the feed port. The coils were optimized for performance at 120.6 MHz, by setting the trap frequency to approximately 260 MHz (coil inductance of 132 nH, total inductance in traps of 36 nH), which is consistent with the values chosen by Schnall et al (Schnall 1985).

Receiver array

The receive array is comprised of 30 dual-tuned rectangular loops on a helmet, with overlapped coils in the head/foot axis forming columns. The width of the loops were selected to maintain a distance between the centers of adjacent columns equal to 130% of the coil width. To maintain uniform column spacing at the top of the former where the radius tapers, two coil sizes were designed. Both coil sizes had a length of 6 cm, and the coil widths were 4 cm and 5 cm. A prototype coil was fabricated and tested (dual-tune/match, detune) using copper tape before sending the coil layout for production as a flexible printed circuit board (PCB).

In order to reduce the number of iterations for coil optimization per element (tune, match, detune and preamp-decouple), the coil former was populated with empty PCB's to approximate the coil positions, and one coil of each size was dual-tuned and placed at each coil position to determine the resonant frequency and loaded Q for each position.

From this procedure, four matching conditions were determined to be sufficient, namely a heavy load and light load for each of the coil sizes. in order to optimise the effectiveness of diode detuning for each frequency, active detuning was implemented for the proton frequency, while the phosphorus frequency was passively detuned as shown in Figure 1c.

Dual-tuning was achieved by replacing the capacitors of a standard coil with dual-tuned Foster network units (a capacitor in series with a parallel inductor and capacitor[9, 10]) in order to give the desired equivalent capacitance at each frequency. The coils were optimized for performance at 120.6 MHz, with an expected SNR penalty of less than 10% for ^{31}P and approximately 30% for ^{1}H. The position and placement of common-mode suppressing cable traps was determined experimentally by measuring the common-mode currents using a current injector and current meter as described by Seeber *et al.*[11], resulting in the use of wire-wound cable traps tuned to the 298 MHz at the feed port of each coil and the use of ceramic floating cable traps for 120.6 MHz in the interface box housing.

2.2 | Phantom and volunteer scans

All scans were performed on a Siemens Magnetom 7T whole body MR system (Siemens Healthcare, Erlangen, Germany). Apart from the previously described array coil, a dual-tuned quadrature birdcage coil from Quality Electrodynamics (Ohio, USA) was also used as a reference, to determine how SNR was affected by the use of the array coil. Both coils are shown in figure 1. Apart from the channel combination steps in processing, both coils were used with identical settings and protocols.

[Figure 1 about here.]

[Table 1 about here.]

Phantom

A 2 l spherical flask was filled with a 16 mM solution of potassium phosphate buffer (pH=7.2) for use as a phantom. This flask reasonably approximates the size and shape of a human head and largely filled the coils' sensitive volumes. Flip angle calibration was performed manually by varying the supplied RF power for a single pulse acquire sequence to find the power giving the maximum amplitude for the phosphate peak, which corresponds to a 90°excitation. A TR of 15s was used to ensure complete relaxation. The ^{31}P MRSI was acquired using a standard 3D pulse acquire CSI sequence with the following parameters: FOV= $200 \times 200 \times 200\,\mathrm{mm}^3$, matrix size= $16 \times 16 \times 16$, TR/TE=1000 ms/2.3 ms, flip angle=30°, spherically sampled k-space for a total acquisition time of 23 minutes. To test the ^{1}H performance of the coil, a similar sequence was run, but with a reduced TR of 200ms due to the shorter T1, and a correspondingly reduced flip angle of 25°. To calibrate the ^{1}H B1 a 3DREAM sequence was used to measure the flip angle from a 1 ms pulse at a selected voltage, this was then scaled to give a 180 °pulse. As a comparison for the ^{1}H performance we chose to use a 32 channel receive array coil from Nova Medical (Massachusetts, USA), as this is a commonly used coil for 7T imaging, rather than the QED birdcage. For these tests we used a 180mm diameter spherical gel phantom.

In vivo

Three healthy volunteers were scanned after giving written informed consent. The School of Psychology, Cardiff University Ethics Committee approved this study. In each case the same scan procedure was followed: after initial B_0 shimming, a 3D T_1-weighted image was acquired with the MPRAGE (magnetization prepared rapid acquisition gradient echo) sequence. This was used to position the ^{31}P excitation slab: in two subjects, the chosen slab was axial through the center of the brain, while for the third a more coronal slab was used, passing through the occipital cortex. .

Once the slab position was chosen, the B_1 transmit power was calibrated in the same way as for the phantom, but this time using a slice selective excitation to ensure the flip angle was optimized for the chosen slab. The MRSI data was acquired with a 2D, slice-selective pulse acquire CSI sequence with the following parameters: FOV= $200 \times 200 \times 40\,\mathrm{mm}^3$, matrix size= 12×12, TR/TE=1000 ms/2.3 ms, BW/NP=10 kHz/4096, flip angle=45°, elliptically weighted k-space sampling with 60 averages at k-space center for a total acquisition time of 24 minutes.

2.3 | Data Processing and Analysis

For each dataset, as a first step a noise profile was created using the last 100 points of every acquired FID, and used to create a whitening transform which removed any noise correlation between individual channels[12]. Next, all k-space points with more than one acquired average were combined in to a single FID.

As the optimal channel combination weights vary spatially all data was first Fourier transformed in the spatial dimensions. Four different methods were then used to combine the channels into a single FID :

- weighted by first point[13]: FIDs from each channel were zero-order phased to make the first point real, then scaled by the (normalized) magnitude of the first point.
- WSVD[12] (Whitened Singular Value Decomposition): the rank-1 truncation of the singular value decomposition was used to obtain the maximum likelihood estimate of the optimal channel weights.
- WSVD+Apod[14]: FIDs were apodized to emphasize the high SNR early part of the signal.
- WSVD+Apod+Blur[14]: In addition to the apodization described above, spatial smoothness was imposed across neighboring voxels before applying the WSVD method.

The performance of all data driven channel combination methods is heavily dependent on the initial SNR for the individual channels. For our acquisitions *in vivo*, we deliberately acquired a relatively large number of averages (60) in order to increase the SNR and improve the calculation of the channel weightings. However, this also extends the exam time substantially (in this case to 24 minutes). In order to evaluate the effect of reducing the scan time on the channel combination, we created simulated datasets for both 30 average (12:40 minutes) and 15 average (6:35 minutes) exams by sub-sampling from the complete 24 minute exams, while maintaining the elliptically weighted k-space sampling.

After channel combination the noise level of each voxel was measured from the standard deviation of the last 500 (complex) points of the FID, and the signal scaled to make this 1. Although all data was acquired using pulse-acquire sequences, the small delay between excitation and readout required by the rewinding of the slice-selective gradient, and the MRSI phase encoding gradient pulses, introduces a systematic first order phase shift into the data, and when this is corrected a baseline distortion is created.

Next the per-voxel zero order phases were determined by minimizing the difference between the magnitude and the real part of the spectra. No further first order phase correction was found to be necessary. For the phantom data, which contains only a single peak, the signal was calculated by a simple integration of the area under the peak. For the *in vivo* data, the phased signal was fitted in the time domain using an AMARES[15] approach using a basis set consisting of the following metabolite peaks: phosphocreatine (PCr), α-, β– and γ-ATP (adenosine triphosphate), inorganic phosphate (Pi), phosphoethanolamine (PEtn), glycerophosphoethanolamin (GPEtn), phosphocholine (PC), glycerophosphocholine (GPC) and nicotinamide adenine dinucleotide (NAD). As the baseline distortion only affects the first few points of the signal, these were excluded from the fitting. The fitted line was subtracted from the original signal to leave only the baseline and noise components, to which a spline was fitted in the frequency domain to obtain a smoothed baseline estimate.

All data processing was done in Python using the Suspect library[16]. The analysis of each dataset was performed in a Jupyter notebook environment and the complete code used for the analysis and all results are published on figshare[17, 18, 19, 20, 21].

3 | RESULTS

The Q factors for the array coil are shown in table 1, for both nuclei and with the coil in a loaded and unloaded state. The S11 values on resonance for the ^{1}H birdcage were -10.26dB and -14.03dB, while for the ^{31}P birdcage the values were -12.83dB and -13.12dB. Transmit power for the ^{31}P was found to be roughly similar to the QED birdcage, with a measured transmitter reference voltage of around 450V. However, the estimated ^{1}H transmit voltage was around 1000V, well above the maximum deliverable voltage of 550V, and much higher than the Nova coil which measured a reference voltage of 194V. During these initial measurements an issue was identified with the ^{1}H quadrature splitter board, which meant that the birdcage could only be driven in a linear mode and on one port, leading to a fourfold reduction in delivered power.

[Table 2 about here.]

3.1 | Phantom measurements

Noise covariance matrices for the array coil from multiple exams are shown in figure 2. The channel loading patterns are similar in each case, with some minor correlation between a few elements. The application of a whitening transform is sufficient to remove all correlations and ensure equal loading of the elements.

The ^{31}P signal to noise maps for central slices of the phantom are shown in figure 3. The full 3D SNR maps are online as Supporting Information Figure S1 As expected, the QED birdcage coil shows very homogeneous SNR across the entire volume of the phantom. By contrast, the array coil is highly heterogeneous, with the highest signals coming from the periphery of the phantom, particularly in the posterior half. In the center of the phantom, signal from the array coil is around 1.2x relative to the QED birdcage, while the maximum SNR enhancement at the edge of the phantom is more than 8x.

[Figure 2 about here.]

Across the whole 3D volume, there are some regions of the phantom where the array coil records no signal at all. These are particularly located in the anterior region at the base of the coil, which is unsurprising as this is the open part of the coil, around the subject's mouth and jaw, where there are no receive elements located. The sharp-eyed will also notice a small region of reduced sensitivity at the anterior of the top of the coil, this is due to a small gap in the coil coverage to allow access for an EEG cap cable. These missing signal regions have no practical consequences for *in vivo* imaging as they fall outside the brain volume.

The equivalent maps for ^{1}H are shown in figure 4. In general the Nova coil shows a somewhat higher SNR than our new coil. For the central region with generally lower sensitivity, the novel coil has on average 60% of the Nova SNR. Both coils display increasing sensitivity towards the periphery, with the Nova coil in particular showing very substantial SNR improvements in the left, right and superior directions. The novel coil has a less pronounced but more symmetric improvement in sensitivity, leading it to offer superior SNR in the anterior and posterior regions of the phantom. Overall, the novel coil has greater sensitivity than the Nova coil in approximately 20% of voxels.

[Figure 3 about here.]

[Figure 4 about here.]

3.2 | Measurements *in vivo*

In our volunteer scans we were able to successfully acquire MRSI of excellent spectral quality using both coils. The ^{31}P transmit power of both coils was very similar, with a measured transmitter reference voltage of approximately 450 in each case. The performances of the different channel combination methods considered are given in figure 5. The traditional first point based method achieved the lowest combined SNR, with the WSVD method having a median of 40-50% more SNR in the 60 average case. With a smaller number of averages (and a lower baseline SNR) WSVD performs relatively better, with a median increase in SNR of 77%.

[Figure 5 about here.]

Adding apodization to the WSVD method produces some additional improvements in SNR, around 5-25% depending on number of averages. There is also a large increase in maximum SNR by using apodization, as this technique is able to correctly combine a small number of problem voxels where WSVD alone struggles. Interestingly, no gain in SNR was seen by using the spatial smoothing constraints of WSVD+Apod.+Blur, the results are almost identical to the simpler WSVD+Apod. method.

The spatial distribution of receiver SNR for the different methods, as well as for the QED birdcage coil, are shown in figure 6. The pattern is very similar to that observed for the phantom, with the QED birdcage showing a largely uniform sensitivity, while the array coil roughly matches performance in the center and has a substantially brighter periphery. In the example shown there is a clear asymmetry with the right hand side of the slice having considerably higher SNR than the left. This is most probably due to minor variation in subject positioning, the very sharp SNR gradients of the individual receive elements makes the peripheral region very sensitive to these kind of small changes.

[Figure 6 about here.]

The acquisition volumes and some representative spectra using the WSVD+Apod.+Blur method are shown in figure 7. For the occipital acquisition (volunteer 3), SNR from the array coil was universally higher than from the QED birdcage, increasing from about 120% in the center of the slab to more than 800% in some peripheral voxels. By contrast, in the two transverse exams, SNR for the array in the center was only 80% of the QED birdcage, rising to around 600% at the edge of the brain.

[Figure 7 about here.]

We were able to reliably quantify all 10 metabolites in our fitting basis set. The β-ATP peak is only partially excited due to insufficient bandwidth on the excitation pulse, and is not considered further, but concentration maps of the other metabolites are shown in figure 8, for both the array coil and QED birdcage. Similar spatial variations in the maps are apparent in both. The α-ATP concentration estimate is slightly reduced relative to the γ-ATP estimate, this is due to the chemical shift artifact: as the excited α-ATP slice is higher in the head, the partial volume effect is increased.

[Figure 8 about here.]

4 | DISCUSSION

In this work we have described a novel coil setup for acquiring whole head ^{31}P data at 7T. The setup features two birdcage volume coils for B_1 transmit at ^{1}H and ^{31}P frequencies respectively, and a dual-tuned 30 channel receiver array. The increase in sensitivity from the use of local receive coils significantly improved the achievable SNR of ^{31}P MRSI in the periphery of the brain, while maintaining signal in the center of the brain.

Avdievich and Hetherington were the first researchers to combine a dual-tuned volume coil for excitation with a phased array for receive[22]. At 4T they used a 4 element array to obtain SNR improvements of 15% in the center of the coil, increasing to 4x at the periphery. However, their receive array was ^{31}P only, all ^{1}H images were acquired using the dual-tuned volume coil.

Subsequently, van de Bank *et al.* improved upon this design at 7T by combining an 8 channel transceiver array for ^{1}H with a ^{31}P transmit volume coil and a 7 channel local receiver array positioned at the back of the coil[6]. In phantom measurements, the array achieved a 7x increase in SNR at the periphery, with SNR improvements up to 7 cm inside the phantom. This agrees well with the performance of our system, which achieved a peak SNR increase of 8x in phantom, however by increasing the number of receiver elements in the array to 30, the new design is able to achieve whole brain coverage with improved SNR.

In comparison to other dual-tuned RF coils following a similar circuit design (as originally described by Schnall et al.[10]), our coil setup uses the same conductors for receiving both ^{1}H and ^{31}P signals. This is in contrast to nested[23] or composite[24] designs, which require double the number of coil elements, complicating the mechanical design. Another design that makes use of the same coil elements for both nuclei uses PIN diodes to switch in an extra capacitor in tuning the coils[25]. It should be noted though that these PIN diodes will substantially affect the unloaded Q, and will therefore likely have lower SNR than the dual-tuned design in our setup.

The performance of data driven channel combination methods such as the WSVD family is dependent upon sufficient SNR as shown by Rodgers and Robson[14]. In our phantom measurements SNR in the center of the volume was around 20% higher with the array coil than the QED birdcage, while in the volunteer exams through the center of the brain (volunteers 1 and 2) the array coil SNR dropped instead to 20% lower than the QED birdcage. Our initial assumption was that this was due to the relatively lower SNR achieved *in vivo* leading to a suboptimal coil combination, and that a superior choice of coil weightings would lead to performance *in vivo* matching the phantom results.

If this were true, we would also expect that the sub-sampled datasets with fewer averages, which have an intrinsically lower SNR, would then suffer from even worse channel combination, leading to a correspondingly lower final SNR. However this is not the case. In Supporting Information Figure S2 maps of the ratio of SNR between the 15 and 30 average cases and the 60 average case for volunteer 1 (combined using the WSVD+Apod.+Blur method). These maps are extremely uniform, with no degradation in performance in the center of the FOV. This strongly suggests that the SNR is sufficient for optimal channel combination, and other factors are responsible for the reduced performance of the array coil in our *in vivo* studies, compared to the phantom exams.

In the imaging domain, the preferred method of channel combination in the low SNR case is the adaptive combine method[26, 27]. This is similar in many ways to the WSVD+Apod+Blur method considered here, a correction is applied to remove any noise correlations between coil elements, and then the signals from a block of neighbor voxels are used to assess the local SNR for each element. In our case, however, we find that there is almost no improvement from adding the Blur component to the WSVD+Apod. This is because with spectroscopy data, we have access to many more data points at each spatial voxel, which already behaves in a similar way to the neighbor block in the adaptive combine method. On top of this, the spectroscopy voxels are much larger than typical imaging voxels, so there is less similarity in channel weightings between neighbors. It may be that when pushing the voxel size smaller, which will naturally reduce

SNR, we see more improvement from the WSVD+Apod+Blur case.

It is standard practice when acquiring spectroscopy data to obtain multiple averages, repeated identical acquisitions which are averaged together to achieve a $\sqrt{N}$ increase in SNR, where N is the number of averages. It is increasingly being realized in single voxel spectroscopy, and particularly for editing sequences, that shifts in B_0 during the acquisition will cause individual averages to become misaligned, adversely affecting the final spectral quality[28, 29]. Before combination, therefore, individual averages should be re-aligned, with the current preferred method being Spectral Registration[30].

Spectral Registration requires a certain level of SNR in order to be effective. In the standard ^{1}H SVS case, channel combination can be done first, greatly improving the performance of the method. However, for MRSI the channel combination can only be done after Fourier transform, while the averaging must happen before. In addition, the intrinsically lower signal from ^{31}P acquisitions means that aligning averages in this way is impractical, often reducing the quality of alignment rather than improving it. For this reason, it was not possible to apply such frequency correction in this study. A greatly preferable approach that should be considered for the future would be to use an interleaved ^{1}H signal to track the B_0 frequency, this would provide plenty of signal to correct any frequency shifts without impacting on the ^{31}P signal[31, 32]. Unfortunately there are for the moment software restrictions within the current Siemens 7T pulse sequence environment which prevent interleaving multi-nuclear receive, this will need to be resolved for progress to be made on this issue.

One of the major challenges with ^{31}P spectroscopy is localizing signal. Due to the very short T2s of the metabolites of interest, conventional techniques such as PRESS or LASER have prohibitive signal losses. The ISIS technique has been used to localize ^{31}P[33], however its heavy use of adiabatic pulses substantially increases the SAR burden and its eight acquisition cycle makes it too long for use with MRSI techniques. The most popular approach is to simply use a slice selective pulse-acquire sequence, using phase encoding to localize the signal. The issue here is that the field of view must fully cover the imaged volume, so it is difficult to achieve small voxel sizes without very long scan times.

With their local receiver array, van de Bank *et al.* were able to exploit the reduced field of view to obtain 3.0 cm^3 voxels in only 15 minutes of scan time[6]. By contrast the novel array coil described here has a whole head field of view, which allows greater flexibility in choice of imaging location, but requires a more difficult trade-off between acquisition time and voxel size. However, the large number of receiver coils permitted by this dual tuned design means that there is considerable potential to make use of techniques such as GRAPPA[34, 35], which undersample data in k-space, and untangle the resulting spatial overlap using the differences in receive element sensitivity maps. This should certainly be a priority for future research in this area.

Currently, a complete assessment of the ^{1}H performance of the novel coil has been hampered by issues with the ^{1}H birdcage, which can only be driven in a linear mode and with a very limited B_1^+. However as figure 4 shows, the sensitivity of the receive array is around 60% of the commonly used Nova coil in the centre of the FoV, and with increasing sensitivity all around the periphery. This means that it is certainly sufficient to provide e.g. ^{1}H localization images to accompany ^{31}P MRSI data, and we anticipate that planned improvements to the birdcage component will improve this performance by giving a greater and more homogeneous B_1^+.

ACKNOWLEDGEMENTS

We gratefully acknowledge the assistance of Alison Paul and Craig James in the preparation of phantoms. RGW thanks the Higher Education Funding Council for Wales. We acknowledge the generous support of the UK Medical Research Council (MR/M008932/1), the Welsh Government and Cardiff University for the CUBRIC ultra-high field imaging facility and associated researchers (BCR). We would like to thank Wellcome for supporting this work: Wellcome

Strategic Award, 'Multi-scale and multi-modal assessment of coupling in the healthy and diseased brain', grant reference 104943/ Z/14/Z (RGW and MT).

REFERENCES

[1] Rowland B, Merugumala SK, Liao H, Creager MA, Balschi J, Lin AP. Spectral improvement by fourier thresholding of in vivo dynamic spectroscopy data. Magnetic Resonance in Medicine 2015 Oct;76(3):978–985.

[2] Meyerspeer M, Robinson S, Nabuurs CI, Scheenen T, Schoisengeier A, Unger E, et al. Comparing localized and nonlocalized dynamic 31P magnetic resonance spectroscopy in exercising muscle at 7T. Magnetic Resonance in Medicine 2012 Feb;68(6):1713–1723.

[3] Paling D, Golay X, Wheeler-Kingshott C, Kapoor R, Miller D. Energy failure in multiple sclerosis and its investigation using MR techniques. Journal of Neurology 2011 Jun;258(12):2113–2127.

[4] Hetherington HP, Kim JH, Pan JW, Spencer DD. 1H and 31P spectroscopic imaging of epilepsy: spectroscopic and histologic correlations. Epilepsia 2004;45 Suppl 4(s4):17–23.

[5] Rodgers CT, Clarke WT, Snyder C, Vaughan JT, Neubauer S, Robson MD. Human cardiac 31P magnetic resonance spectroscopy at 7 tesla. Magnetic Resonance in Medicine 2013 Sep;72(2):304–315.

[6] van de Bank BL, Orzada S, Smits F, Lagemaat MW, Rodgers CT, Bitz AK, et al. Optimized 31P MRS in the human brain at 7 T with a dedicated RF coil setup. NMR in Biomedicine 2015 Oct;28(11):1570–1578.

[7] van der Velden TA, Italiaander M, van der Kemp WJM, Raaijmakers AJE, Schmitz AMT, Luijten PR, et al. Radiofrequency configuration to facilitate bilateral breast 31P MR spectroscopic imaging and high-resolution MRI at 7 Tesla. Magnetic Resonance in Medicine 2014 Dec;74(6):1803–1810.

[8] Fitzsimmons JR, Beck BL, Brooker HR. Double resonant quadrature birdcage. Magnetic Resonance in Medicine 1993 Jul;30(1):107–114.

[9] Meyerspeer M, Roig ES, Gruetter R, Magill AW. An improved trap design for decoupling multinuclear RF coils. Magnetic Resonance in Medicine 2013 Sep;72(2):584–590.

[10] Schnall MD, Subramanian VH, Leigh JS, Chance B. A new double-tuned probed for concurrent 1H and 31P NMR. Journal of Magnetic Resonance (1969) 1985;65(1):122–129.

[11] Seeber DA, Jevtic J, Menon A. Floating shield current suppression trap. Concepts in Magnetic Resonance Part B: Magnetic Resonance Engineering 2004;21B(1):26–31.

[12] Rodgers CT, Robson MD. Receive array magnetic resonance spectroscopy: Whitened singular value decomposition (WSVD) gives optimal Bayesian solution. Magnetic Resonance in Medicine 2010 May;63(4):881–891.

[13] Brown MA. Time-domain combination of MR spectroscopy data acquired using phased-array coils. Magnetic Resonance in Medicine 2004 Nov;52(5):1207–1213.

[14] Rodgers CT, Robson MD. Coil combination for receive array spectroscopy: Are data-driven methods superior to methods using computed field maps? Magnetic Resonance in Medicine 2015 Mar;75(2):473–487.

[15] Vanhamme Lea. Improved Method for Accurate and Efficient Quantification of MRS Data with Use of Prior Knowledge 1997 Nov;p. 1–9.

[16] Rowland BC. OpenMRSLab: An open-source software repository for Magnetic Resonance Spectroscopy data analysis tools . In: ESMRMB; 2017. p. 687–688.

[17] Rowland BC, Phantom Analysis; 2018. https://figshare.com/articles/Phantom_Analysis/6791804, (accessed: 09/07/2018).

[18] Rowland BC, Subject 1 Analysis; 2018. https://figshare.com/articles/Subject_1_Analysis/6791882, (accessed: 09/07/2018).

[19] Rowland BC, Subject 2 Analysis; 2018. https://figshare.com/articles/Subject_2_Analysis/6791906, (accessed: 09/07/2018).

[20] Rowland BC, Subject 3 Analysis; 2018. https://figshare.com/articles/Subject_3_Analysis/6791918, (accessed: 09/07/2018).

[21] Rowland BC, Fitting Model Parameters; 2018. https://figshare.com/articles/Fitting_Model_Parameters/6791963, (accessed: 09/07/2018).

[22] Avdievich NI, Hetherington HP. 4T Actively detuneable double-tuned 1H/31P head volume coil and four-channel 31P phased array for human brain spectroscopy. Journal of Magnetic Resonance 2007 Jun;186(2):341–346.

[23] Brown R, Madelin G, Lattanzi R, Chang G, Regatte RR, Sodickson DK, et al. Design of a nested eight-channel sodium and four-channel proton coil for 7T knee imaging. Magnetic Resonance in Medicine 2012 Aug;70(1):259–268.

[24] Kaggie JD, Hadley JR, Badal J, Campbell JR, Park DJ, Parker DL, et al. A 3 T sodium and proton composite array breast coil. Magnetic Resonance in Medicine 2013 Sep;71(6):2231–2242.

[25] Ha S, Hamamura MJ, Nalcioglu O, Muftuler LT. A PIN diode controlled dual-tuned MRI RF coil and phased array for multi nuclear imaging. Physics in Medicine and Biology 2010 Apr;55(9):2589–2600.

[26] Walsh DO, Gmitro AF, Marcellin MW. Adaptive reconstruction of phased array MR imagery. Magnetic Resonance in Medicine 2000 May;43(5):682–690.

[27] Benkhedah N, Hoffmann SH, Biller A, Nagel AM. Evaluation of adaptive combination of 30-channel head receive coil array data in 23Na MR imaging. Magnetic Resonance in Medicine 2015 Mar;75(2):527–536.

[28] Rowland BC, Liao H, Adan F, Mariano L, Irvine J, Lin AP. Correcting for Frequency Drift in Clinical Brain MR Spectroscopy. Journal of Neuroimaging 2016 Sep;27(1):23–28.

[29] Harris AD, Glaubitz B, Near J, John Evans C, Puts NAJ, Schmidt-Wilcke T, et al. Impact of frequency drift on gamma-aminobutyric acid-edited MR spectroscopy. Magnetic Resonance in Medicine 2013 Nov;72(4):941–948.

[30] Near J, Edden R, Evans CJ, Paquin R, Harris A, Jezzard P. Frequency and phase drift correction of magnetic resonance spectroscopy data by spectral registration in the time domain. Magnetic Resonance in Medicine 2014 Jan;73(1):44–50.

[31] Bhattacharyya PK, Lowe MJ, Phillips MD. Spectral quality control in motion-corrupted single-voxel J-difference editing scans: An interleaved navigator approach. Magnetic Resonance in Medicine 2007;58(4):808–812.

[32] Keating B, Ernst T. Real-time dynamic frequency and shim correction for single-voxel magnetic resonance spectroscopy. Magnetic Resonance in Medicine 2012 Jan;68(5):1339–1345.

[33] van Sluis R, Yongbi NM, Payne GS, Leach MO. Simultaneous localized 1H STEAM/31P ISIS spectroscopy in vivo. Magnetic Resonance in Medicine 1996 Apr;35(4):465–470.

[34] Santos-Díaz A, Obruchkov SI, Schulte RF, Noseworthy MD. Phosphorus magnetic resonance spectroscopic imaging using flyback echo planar readout trajectories. Magnetic Resonance Materials in Physics, Biology and Medicine 2018 Jan;p. 1–12.

[35] Zhu X, Ebel A, Ji JX, Schuff N. Spectral phase-corrected GRAPPA reconstruction of three-dimensional echo-planar spectroscopic imaging (3D-EPSI). Magnetic Resonance in Medicine 2007;57(5):815–820.

[36] Haase A, Odoj F, Von Kienlin M, Warnking J, Fidler F, Weisser A, et al. NMR probeheads for in vivo applications. Concepts in Magnetic Resonance Part A 2000 Jan;12(6):361–388.

LIST OF FIGURES

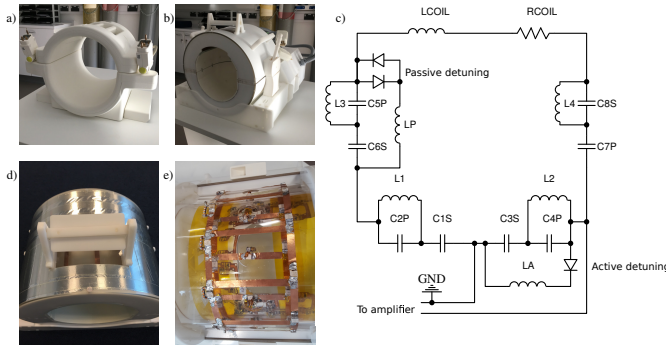

FIGURE 1 The two head coils used in this study: a) the novel 30 channel receiver array coil from MR Coils (Zaltbommel, Netherlands); b) standard single channel birdcage coil from Quality Electrodynamics (Ohio, USA); c) circuit diagram for a single receive loop of the dual tuned receive array; d) a gap in the coil shielding allows the subject to see out of the coil; e) the two layers of the transmit birdcage.

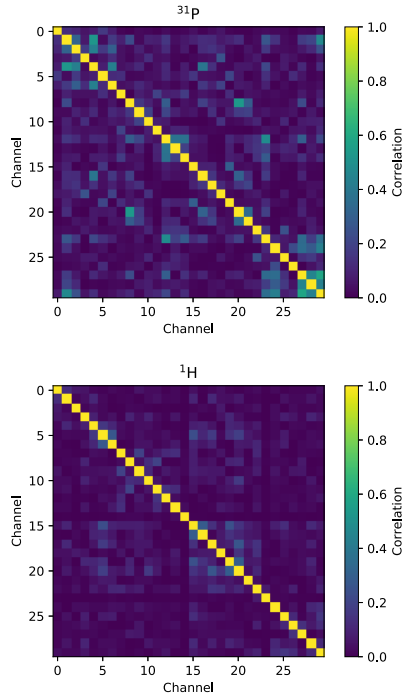

FIGURE 2 Noise correlation matrices from the 30 channel receive array. The ^{31}P data (top) was collected from subject 1, while the ^{1}H data (bottom) was obtained from a gel phantom.

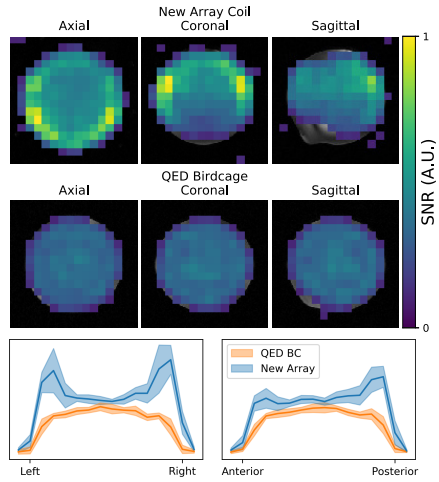

FIGURE 3 ^{31}P SNR maps from the new array coil and the QED birdcage coils in phantom. Below we show for each coil cross sections of the mean sensitivity profiles (±1 standard deviation) calculated from the central 4x4 block of rows in the left-right and anterior-posterior directions. The QED birdcage coil provides excellent uniform, flat coverage of the whole volume, while the array coil has some gaps in sensitivity, particularly in the inferior-anterior region, where there are no receive elements. However the array coil provides substantially increased signal across the whole field of view, with the greatest improvements in the periphery of the phantom where in some voxels it is 8x higher. Maps covering the whole of the receive volume can be found in the supplementary material.

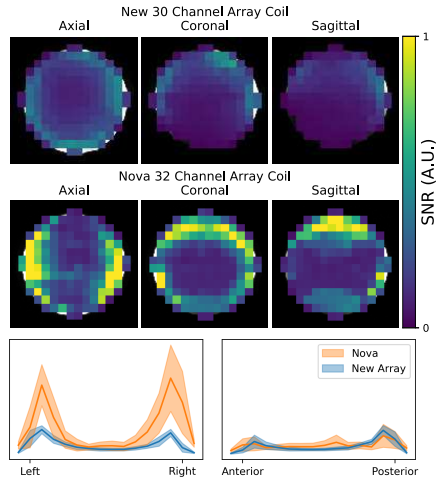

FIGURE 4 ^{1}H SNR maps from the new array coil and Nova coil in phantom. Both coils show the characteristic array coil pattern of lower sensitivity in the centre, increasing towards the periphery. Below we show for each coil cross sections of the mean sensitivity profiles (±1 standard deviation) calculated from the central 4x4 block of rows in the left-right and anterior-posterior directions. The Nova coil shows a relatively greater increase, particularly at the left and right of the volume, while the novel coil has a more circular pattern in the axial plane, giving it higher sensitivity at the anterior and posterior of the phantom. Interestingly the Nova coil appears very sensitive at the extreme caudal edge of the phantom.

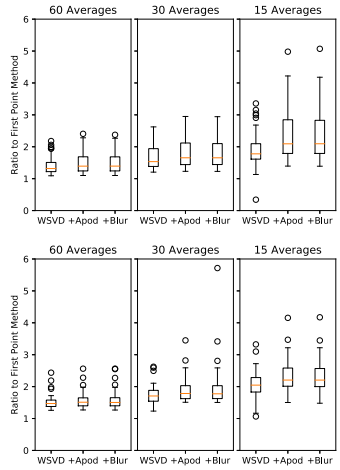

FIGURE 5 Comparison of *in vivo* ^{31}P SNR across channel combination methods. For each of the WSVD based methods and for each size of dataset the phosphocreatine concentration relative to the First Point method were calculated per-voxel. Data is shown for volunteers 1 (top) and 3 (bottom), results from volunteer 2 are similar to volunteer 1 and may be found in the supplementary material.

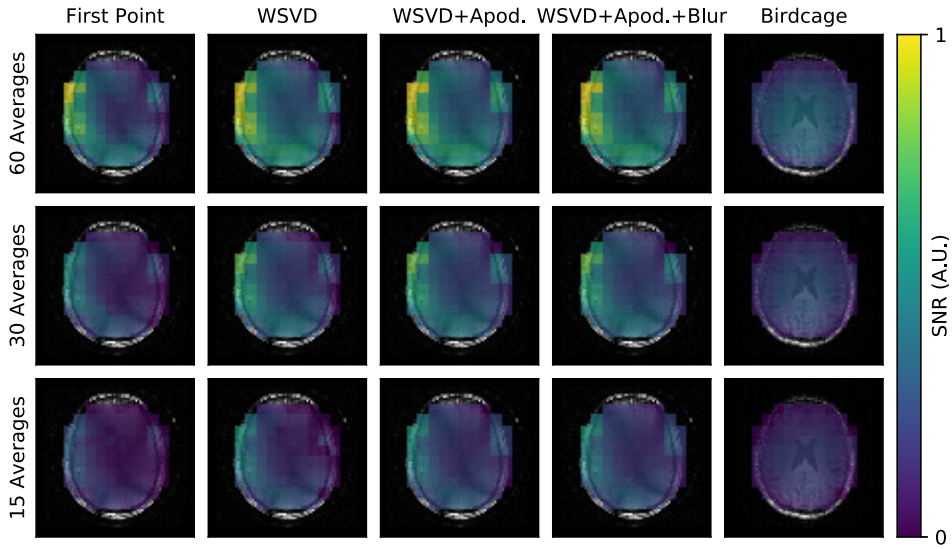

FIGURE 6 SNR maps of the phosphocreatine (PCr) peak acquired from volunteer 1. The top row shows the full dataset (60 averages at k-space center), while the middle and lower datasets are subsampled to simulate shorter acquisitions with 30 and 15 central averages respectively. The first four columns represent different methods for combining the channels of the array coil, while the final column shows the results from the QED birdcage coil. The WSVD methods all give excellent channel combination performance, with essentially no difference between the WSVD+Apod. and WSVD+Apod.+Blur techniques. Localisation images shown below the maps were acquired immediately prior to the MRSI using the corresponding coil and without moving the subject.

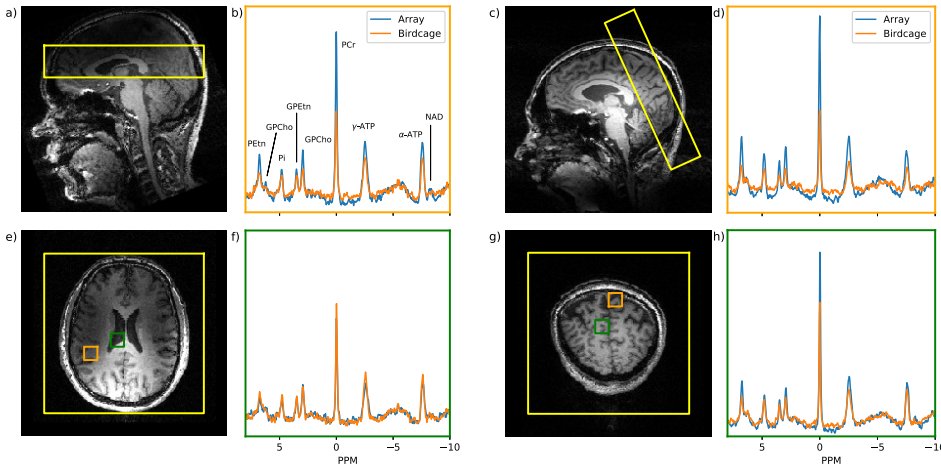

FIGURE 7 Representative ^{31}P spectra from the two coils: a) and c) sagittal view of the subject showing the excited slab in each case; e) and g) slice in the plane of the slab showing example voxels in the center of the brain (red) and in the periphery (purple); b) and d) spectra from peripheral voxels from the array (blue) and QED birdcage (orange) coils; f) and h) spectra from central voxels. All spectra are scaled to have the same noise standard deviation. Localisation images shown below the maps are those acquired by the QED birdcage coil.

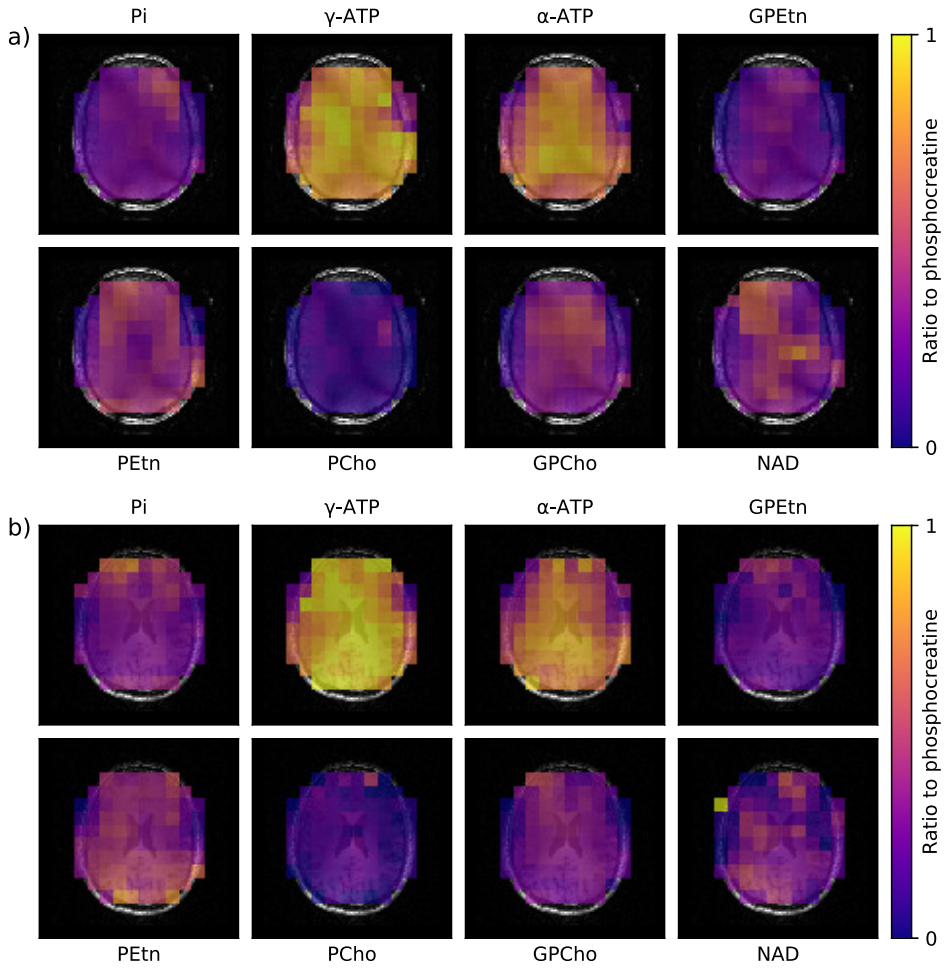

FIGURE 8 Metabolite ratio maps from volunteer 1 using a) the array coil and b) the QED birdcage. Metabolite peaks were fitted from the full 60 average dataset with the WSVD+Apod.+Blur channel combination used for the array data. Because of the highly heterogeneous receiver sensitivity of the array, each metabolite concentration is shown as a ratio to the phosphocreatine peak, which divides out the receiver profiles at the cost of making the maps sensitive to the phosphocreatine distribution. Localisation images shown below the maps were acquired immediately prior to the MRSI using the corresponding coil and without moving the subject.

LIST OF TABLES

TABLE 1 Component values for the circuit diagram in figure 1.

Matching						
C1S	C2P	C3S	C4P	L1	L2	
33+27	33+20	33+27	33+20	5 nH	5 nH	
Tuning						
C6S	C5P	L3	LP	C8S	C7P	L4
30+3.3	30	8 nH	22 nH	30+3.3	30	8 nH

TABLE 2 Measured Q factors for the array coil. Relative coil sensitivity is calculated as $\frac{S}{S_0} = \sqrt{1 - \frac{Q_{\text{loaded}}}{Q_{\text{unloaded}}}}$ [36]

	Q unloaded, single	Q unloaded, dual	Q loaded	Sensitivity, single	Sensitivity, dual
^{1}H	230	140	26	94%	90%
^{31}P	360	210	46	93%	88%